IEEE Access
Multidisciplinary | Rapid Review | Open Access Journal

Received February 23, 2022, accepted March 30, 2022, date of publication April 12, 2022, date of current version April 20, 2022.

Digital Object Identifier 10.1109/ACCESS.2022.3166913

Comparison of First- and Second-Order Sliding-Mode Controllers for a DC-DC Dual Active Bridge

ARNAU DÒRIA-CEREZO[1,2], FEDERICO M. SERRA[3], FRANCISCO D. ESTEBAN[3], DOMINGO BIEL[2,4], AND ROBERT GRIÑÓ[2,5], (Senior Member, IEEE)

[1]Department of Electrical Engineering, Universitat Politècnica de Catalunya, 08034 Barcelona, Spain
[2]Institute of Industrial and Control Engineering, Universitat Politècnica de Catalunya, 08034 Barcelona, Spain
[3]Laboratorio de Control Automático (LCA), Facultad de Ingeniería y Ciencias Agropecuarias, Universidad Nacional de San Luis—CONICET, Villa Mercedes, San Luis 5730, Argentina
[4]Department of Electronic Engineering, Universitat Politècnica de Catalunya, 08034 Barcelona, Spain
[5]Department of Automatic Control, Universitat Politècnica de Catalunya, 08034 Barcelona, Spain

Corresponding author: Arnau Dòria-Cerezo (arnau.doria@upc.edu)

This work was supported in part by the Government of Spain through the Agencia Estatal de Investigación under Project DPI2017-85404-P, and in part by the Generalitat de Catalunya under Project 2017 SGR 872.

ABSTRACT This paper compares four sliding-mode control strategies for a dual active bridge. The proposed control algorithms define different switching functions resulting in first-and second-order controllers, and using both discontinuous and continuous sliding-mode algorithms. The paper details the design stage and includes simulation and experimental tests to better compare the performance for each control scheme.

INDEX TERMS Dual active bridge, discontinuous sliding-mode controllers, continuous sliding-mode controllers.

I. INTRODUCTION

The dual active bridge (DAB) is a power converter widely used in several applications such as microgrids [1], [2], electric vehicles [3], aeronautic field (the so-called More Electric Aircraft, MEA) [4], energy storage systems [5], solid-state transformer in medium-voltage and low-voltage distribution networks [6], among others. The main features of DAB converters are high power density, bidirectional power flow, galvanic isolation, and the possibility of soft switching [7].

The DAB has two active bridges interconnected with a high-frequency transformer. The model of the DAB converter results in a nonlinear switched dynamical system that mixes two dc stages (input and output) with an ac stage in between due to the magnetic transformer. Usually, the switched model is averaged based on the power flowing between the two ports resulting in first-order nonlinear dynamics for the output voltage. See [8] for a detailed discussion on this behavioural modelling.

From the averaged model, most of the approaches devoted to the control of DAB propose a linearization around a working point and use standard linear techniques such as PI controllers [9], phase compensators [10], or linear observers [11]. Alternatively, other works use nonlinear control strategies, including passivity-based techniques [12], [13], discrete-time nonlinear controllers [14], or the feedback linearization approach [15], [16]. Sliding-mode controllers (SMC) have also been proposed for the control of DAB, including a first-order design [17], the double integral sliding-mode control [18], and the super-twisting algorithm [4]. The main properties of SMC are finite-time stabilization, the robustness in front of parametric uncertainties, and the rejection of disturbances. The SMC designs mentioned above, and most of the control designs available in the literature, propose a change of variables increasing the algorithm complexity, or approximations to overcome the strong nonlinearity in the control input function.

This paper offers a different alternative: to transform the system into an affine form with the control input via a dynamic extension. From the extended model, four different sliding-mode strategies are compared; the classical First-Order (FO) sliding-mode controller, the Twisting-Algorithm (TA), the Super-Twisting Algorithm (STA), and the Discontinuous Integral Controller (DIC). These strategies include both Discontinuous Sliding-Mode Controllers (DSMCs) and Continuous Sliding-Mode Controllers (CSMCs). In DSMCs,

The associate editor coordinating the review of this manuscript and approving it for publication was Zhuang Xu.

such as FO and TA, the control action is switched, implying undesired oscillations (known as the chattering phenomena). The STA and DIC strategies are CSMCs developed to reduce the chattering through the replacement of switching functions by continuous ones but retaining some robustness properties and finite-time convergence.

The remainder of the paper is organized as follows. In Section II, the DAB converter is presented, and the dynamical model is obtained. The sliding-mode controllers are defined in Section III, including a description of the design and tuning. Preliminary simulation results to assess the proposed controllers are shown in Section IV and, Section V include the experimental setup description and tests. The overall comparison among the four controllers can be found in Section VI, and, finally, the conclusions are stated in Section VII.

II. DYNAMICAL MODEL

A. THE DUAL ACTIVE BRIDGE CONVERTER

Figure 1 shows a simplified scheme of the DAB converter. It consists of a two-port high frequency transformer with two full-bridge switches connected to each transformer winding, a dc-voltage source, E, in the primary and a capacitor in the secondary side, ports A and B, respectively. The control goal is regulating the dc-voltage capacitor.

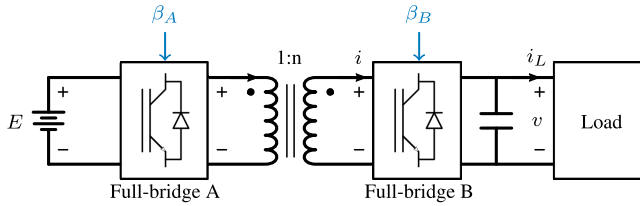

FIGURE 1. Simplified scheme of dual active bridge converter.

Neglecting the magnetizing current of the transformer and considering unity turns ratio, the DAB dynamics can be written as [19]

$$L\frac{\mathrm{d}i}{\mathrm{d}t} = \beta_A E - \beta_B(\delta)v - ri \tag{1a}$$

$$C\frac{\mathrm{d}v}{\mathrm{d}t} = \beta_B(\delta)i - i_L, \tag{1b}$$

where i is the transformer current in the secondary, v is the dc input voltage, i_L is the load current, L is the equivalent inductance, C is the capacitance of the output capacitor, and r represents the transformer losses. All the parameters are referred to the secondary of the transformer. The gate signals β_A, β_B are square wave signals with switching frequency, f_s, and a certain phase-shift, δ. See Figure 2, where $T_s = \frac{1}{f_s}$. A mathematical description of the gate signals is given by

$$\beta_A = \mathrm{sign}(\sin(\omega_s t)) \tag{2a}$$

$$\beta_B = \mathrm{sign}(\sin(\omega_s t - \delta)), \tag{2b}$$

where $\omega_s = 2\pi f_s$. The phase shift, δ, between signals β_A and β_B is used as control input and is updated at every sampled time, T_s.

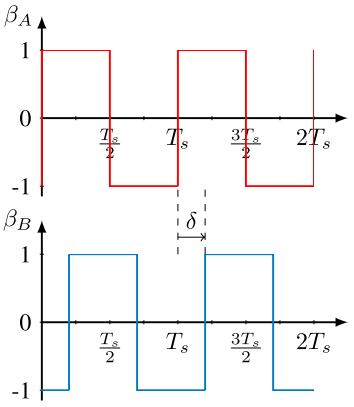

FIGURE 2. Phase shift modulation, according to (2).

B. AVERAGED MODEL AND DYNAMIC EXTENSION

The system (1) is a switched nonlinear system. The switching frequency, f_s, is selected high enough so that the effect of the discontinuous signals β_A and β_B in the capacitor dynamics can be neglected. Thanks to this assumption, averaged models are usually adopted for the control design. Among others, a standard model based on assuming a periodic regime and averaging for the power flowing through the DAB converter is [8]

$$C\frac{\mathrm{d}v}{\mathrm{d}t} = -i_L + \frac{E}{\omega_s L}\delta\left(1 - \frac{|\delta|}{\pi}\right). \tag{3}$$

Assuming a static load composed by a resistor and a constant power load (CPL), the load current can be expressed as

$$i_L = \frac{v}{R_L} + \frac{P_L}{v}, \tag{4}$$

where R_L is the resistance value and P_L is the power consumed by the CPL.

The system (3) is still nonlinear and non-affine with the control input, δ. In the literature two different alternatives are found to attain the control design: linear approximations, or the inversion of the function $\delta\left(1 - \frac{|\delta|}{\pi}\right)$, see [20] or [16], respectively. This work proposes an alternative approach that consists

$$\delta = \int u(t)\mathrm{d}t, \tag{5}$$

where u is the new control input.

Combining (3), (4) and (5), the overall dynamics results in

$$C\frac{\mathrm{d}v}{\mathrm{d}t} = -\frac{v}{R_L} - \frac{P_L}{v} + \frac{E}{\omega_s L}\delta\left(1 - \frac{|\delta|}{\pi}\right), \tag{6a}$$

$$\frac{\mathrm{d}\delta}{\mathrm{d}t} = u. \tag{6b}$$

The control objective is to regulate the average of the capacitor voltage, v, to a desired value, v_d, by acting on the control input u in (6b). Therefore, the system has relative degree two.

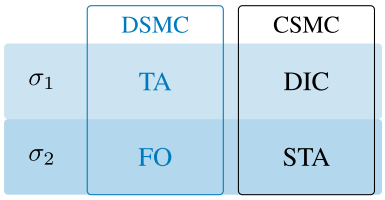

FIGURE 3. Proposed control methods depending on the relative degree of the sliding manifold (σ_1 has relative degree two; σ_2 has relative degree one) and the discontinuous (DSMC) or continuous (CSMC) control actions.

III. SLIDING-MODE CONTROLLERS

When applying SMC for systems of relative degree two, different alternatives exist. A first approach is to define the voltage error as the switching function, i.e.,

$$\sigma_1 = v_d - v, \tag{7}$$

and use a Second-Order Sliding-Mode Controller. Alternatively, the time derivative of the output can be included in the switching function which has relative degree one. For example

$$\sigma_2 = v_d - v - \tau \frac{\mathrm{d}v}{\mathrm{d}t}, \tag{8}$$

where the parameter $\tau > 0$ corresponds to the time constant of the error dynamics once the sliding motion is reached. Notice that assuming, $\sigma_2 = 0$, the voltage dynamics is easily identified as the first order dynamics

$$\frac{v(s)}{v_d(s)} = \frac{1}{\tau s + 1}. \tag{9}$$

The sliding motion in (7) can be enforced applying the Twisting Algorithm (TA) [21]

$$u = -k_{\mathrm{TA},1} \operatorname{sign} \sigma_1 - k_{\mathrm{TA},2} \operatorname{sign} \dot{\sigma}_1. \tag{10}$$

On the other hand, the classical First-Order Sliding-Mode Control (FO) [22]

$$u = -k_{\mathrm{FO}} \operatorname{sign} \sigma_2, \tag{11}$$

achieves sliding motion on (8). Both TA and FO result in discontinuous control actions that imply in oscillations related to the chattering phenomena.

Alternatively, CSMCs are proposed in the literature to reduce the chattering still preserving robustness properties and finite-time response. For systems of relative degree two, the Discontinuous Integral Controller (DIC) is proposed in [23], and it is defined as

$$\begin{aligned} u &= -k_{\mathrm{DIC},1} |\sigma_1|^{1/3} \operatorname{sign} \sigma_1 \\ &\quad -k_{\mathrm{DIC},2} |\dot{\sigma}_1|^{1/2} \operatorname{sign} \dot{\sigma}_1 + \nu_{\mathrm{DIC}} && \text{(12a)} \\ \dot{\nu}_{\mathrm{DIC}} &= -k_{\mathrm{DIC},3} \operatorname{sign} \sigma_1. && \text{(12b)} \end{aligned}$$

For systems of relative degree one, the Super-Twisting Algorithm (STA) [24] is a well-known alternative of CSMCs, and takes the form

$$\begin{aligned} u &= -k_{\mathrm{STA},1} |\sigma_2|^{1/2} \operatorname{sign} \sigma_2 + \nu_{\mathrm{STA}} && \text{(13a)} \\ \dot{\nu}_{\mathrm{STA}} &= -k_{\mathrm{STA},2} \operatorname{sign} \sigma_2. && \text{(13b)} \end{aligned}$$

In this paper the four SMC mentioned above are designed for the voltage regulation of a DAB. Figure 3 shows how the control methods are classified depending on the relative degree and their continuous or discontinuous properties. The corresponding control schemes of the proposed controllers are depicted in Figure 4.

A. THE TWISTING ALGORITHM

The TA uses the switching function in (7). Using (6), the second time derivative of σ_1 can be written as

$$\frac{\mathrm{d}^2\sigma_1}{\mathrm{d}t^2} = \phi + \gamma u, \tag{14}$$

where

$$\begin{aligned} \phi &= \frac{1}{CR_L} + \frac{P_L}{Cv^2} && \text{(15a)} \\ \gamma &= \frac{E(\pi - 2|\delta|)}{\omega_s LC\pi}. && \text{(15b)} \end{aligned}$$

Functions ϕ and γ can be bounded as

$$\begin{aligned} |\phi| < \Phi &= \frac{1}{CR_{L,\min}} + \frac{P_{L,\max}}{Cv_{\min}^2} && \text{(16a)} \\ \gamma \geq \Gamma_m &= \frac{E(\pi - 2\max(|\delta|))}{\omega_s LC\pi} && \text{(16b)} \\ \gamma \leq \Gamma_M &= \frac{E\pi}{\omega_s LC\pi}, && \text{(16c)} \end{aligned}$$

where $R_{L,\min}$, $v_{\min}$ are the minimum values of the load resistance and output voltage, respectively, and $P_{L,\max}$ is the maximum expected value of the CPL. Note that $\delta \in \left(-\frac{\pi}{2}, \frac{\pi}{2}\right)$ is assumed.

From [21], the control parameters can be tuned according to

$$\begin{aligned} k_{\mathrm{TA},1} > k_{\mathrm{TA},2} > 0, && \text{(17a)} \\ \Gamma_m(k_{\mathrm{TA},1} + k_{\mathrm{TA},2}) - \Phi > \Gamma_M(k_{\mathrm{TA},1} - k_{\mathrm{TA},2}) + \Phi, && \text{(17b)} \\ \Gamma_m(k_{\mathrm{TA},1} - k_{\mathrm{TA},2}) > \Phi. && \text{(17c)} \end{aligned}$$

Using the values of the prototype parameters detailed in Table 1, with $R_{L,\min} = 9\ \Omega$, $P_{L,\max} = 108$ W, $v_{\min} = 25$ V, and $\max(|\delta|) = 85°$ (a value close to $\frac{\pi}{2}$), the conditions (17a) and (17c) result in

$$\begin{aligned} k_{\mathrm{TA},1} + k_{\mathrm{TA},2} > 18(k_{\mathrm{TA},1} - k_{\mathrm{TA},2}) + 1.22, && \text{(18a)} \\ k_{\mathrm{TA},1} - k_{\mathrm{TA},2} > 0.61. && \text{(18b)} \end{aligned}$$

B. THE FIRST-ORDER SLIDING-MODE CONTROLLER

In this section a FO sliding-mode controller is designed. Differentiating (8) with respect to time and using (6) one gets

$$\frac{\mathrm{d}\sigma_2}{\mathrm{d}t} = \Psi + \frac{\tau}{C}\gamma u, \tag{19}$$

where, γ is given in (15b) and

$$\Psi = \frac{v + \tau}{CR_L} + \frac{P_L}{Cv} - \frac{E}{\omega_s LC}\delta\left(1 - \frac{|\delta|}{\pi}\right) - \frac{\tau P_L}{Cv^2}. \tag{20}$$

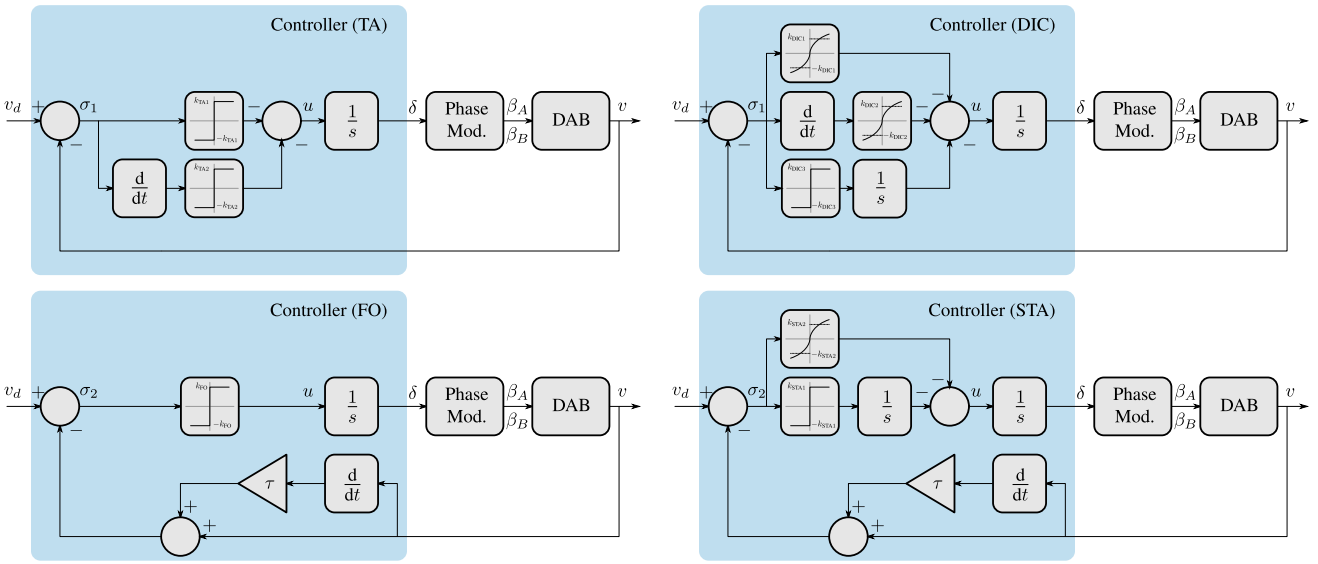

FIGURE 4. Control schemes: the Twisting Algorithm (top left), the First Order SMC (bottom left), the Discontinuous Integral Controller (top right), and the Super-Twisting Algorithm (bottom right).

The equivalent control, u_{eq}, is defined as the control input guaranteeing $\sigma_2 = 0$ and $\dot{\sigma}_2 = 0$. Hence, from (19),

$$u_{eq} = -\frac{C}{\tau\gamma}\Psi. \tag{21}$$

The sliding motion is ensured if the reachability condition, $\sigma_2\dot{\sigma}_2 < 0$, is fulfilled. Using (19) and (21) one can write

$$\sigma_2\frac{\mathrm{d}\sigma_2}{\mathrm{d}t} = -\frac{\tau}{C}\gamma\sigma_2(u_{eq} - u),$$

and replacing the control law (11)

$$\sigma_2\frac{\mathrm{d}\sigma_2}{\mathrm{d}t} = -\frac{\tau}{C}\gamma\sigma_2(u_{eq} + k_{\mathrm{FO}}\,\mathrm{sign}\,\sigma_2), \tag{22}$$

hence the sliding motion is guaranteed if

$$k_{\mathrm{FO}} > |u_{eq}| \tag{23}$$

$$\gamma > 0. \tag{24}$$

The control tuning is based on the first condition. The second condition is ensured since $\delta \in (-\frac{\pi}{2}, \frac{\pi}{2})$.

With the same scenario described in Section III-A with $\max(|\delta|) = 85°$, the sliding motion is guaranteed with

$$k_{\mathrm{FO}} > 36.3654. \tag{25}$$

Notice that large values of k_{FO} imply fastest convergence to σ_2 but higher chattering.

C. THE DISCONTINUOUS INTEGRAL CONTROLLER

Combining (6a)-(6b) with (7) one gets

$$\frac{\mathrm{d}\sigma_1}{\mathrm{d}t} = \xi \tag{26}$$

$$\frac{\mathrm{d}\xi}{\mathrm{d}t} = \frac{1}{C}\left(\frac{1}{R_L} - \frac{P_L}{(\sigma_1 - v_d)^2}\right)\xi + \gamma u, \tag{27}$$

where γ is detailed in (15b).

Assuming small variations of γ, the system (26)-(27) can be seen as a double integrator with a disturbance as requested in [23]. Hence, the DIC with the form (12a)-(12b) stabilize at $\sigma_1 = 0$ in finite time. The selection of the DIC gains follows the procedure given in [23].

D. THE SUPER-TWISTING ALGORITHM

Applying the time derivative of σ_2 in (19) together with (13a)-(13b) results in

$$\frac{\mathrm{d}\sigma_2}{\mathrm{d}t} = \Psi + \frac{\tau}{C}\gamma\left(-k_{\mathrm{STA},1}|\sigma_2|^{1/2}\,\mathrm{sign}\,\sigma_2 + \nu_{\mathrm{STA}}\right) \tag{28a}$$

$$\dot{\nu}_{\mathrm{STA}} = -k_{\mathrm{STA},2}\,\mathrm{sign}\,\sigma_2. \tag{28b}$$

Assuming small variations of γ, the system (28a)-(28b) matches with the perturbed STA. See the gain selection in [25].

IV. SIMULATION RESULTS

Numerical simulations in Matlab-Simulink environment have been carried out to test the proposed controllers.

TABLE 1. DAB parameters.

Symbol	Parameters	Values
C	Output capacitance	940 μF
L	Transformer inductance	38 μH
r	Parasitic loses	0.04 Ω
E	Input voltage	40 V
f_s	Switching frequency	20 kHz

TABLE 2. Control parameters.

Strategy	Controller gains
TA	$k_{\mathrm{TA},1} = 2\cdot 10^3$, $k_{\mathrm{TA},2} = 0.9k_{\mathrm{TA},1}$
FO	$\tau = 5\cdot 10^{-4}$, $k_{\mathrm{FO}} = 5\cdot 10^3$
DIC	$k_{\mathrm{DIC},1} = 2.5\cdot 10^3$, $k_{\mathrm{DIC},2} = 0.95k_{\mathrm{DIC},1}$, $k_{\mathrm{DIC},3} = 10$
STA	$k_{\mathrm{STA},1} = 2.5\cdot 10^3$, $k_{\mathrm{STA},2} = 10$

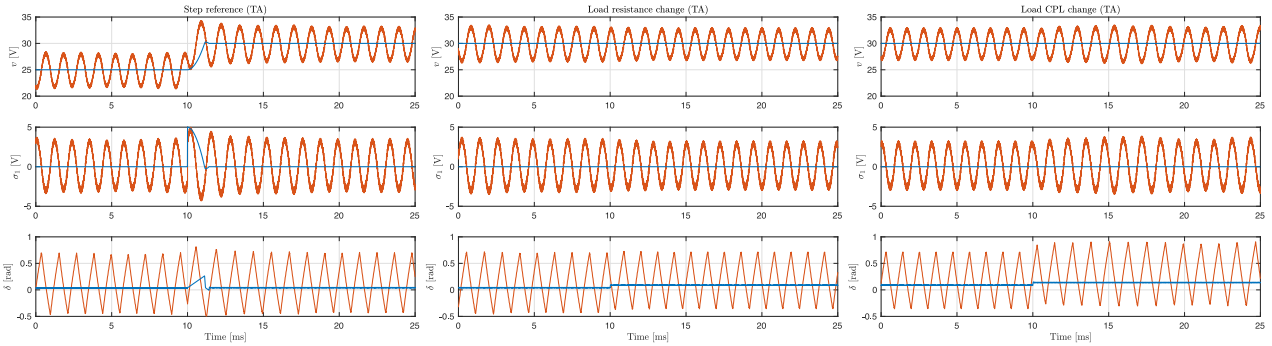

FIGURE 5. Simulation results for the Twisting Algorithm (TA): Averaged model (blue), switched model (red). Reference change (left), resistive load change (center), and CPL change (right). Output voltage (top), switching manifold (mid), and phase-shift control signal (bottom).

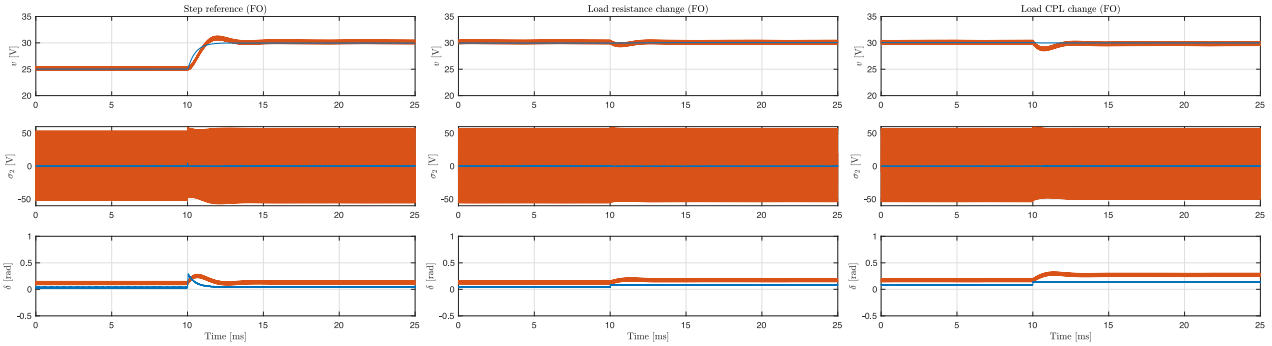

FIGURE 6. Simulation results for the First-order sliding-mode controller (FO): Averaged model (blue), switched model (red). Reference change (left), resistive load change (center), and CPL change (right). Output voltage (top), switching manifold (mid), and phase-shift control signal (bottom).

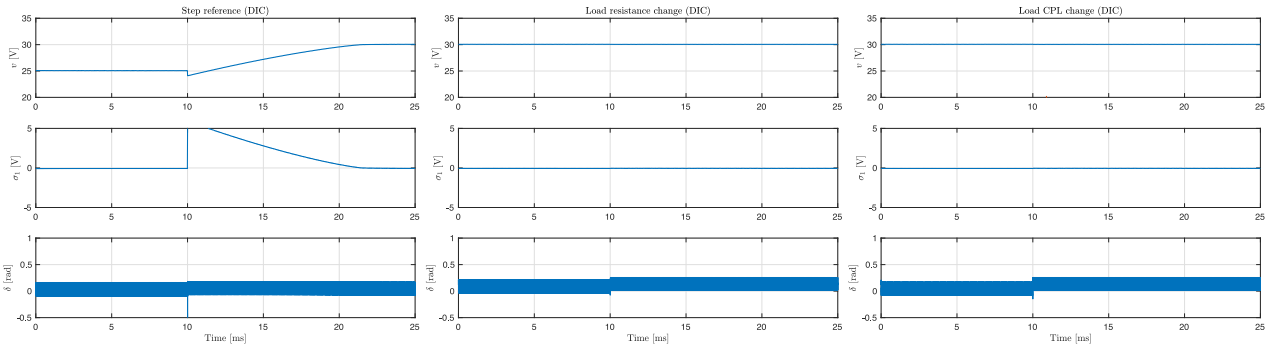

FIGURE 7. Simulation results for the Discontinuous Integral Controller (DIC): Averaged model (blue), switched model (red). Reference change (left), resistive load change (center), and CPL change (right). Output voltage (top), switching manifold (mid), and phase-shift control signal (bottom).

The performance of the controllers has been compared under the averaged model (3) and the switched model (1a)-(1b) that contains the sampling period, T_s, associated to the switching signals β_A, β_B. The parameters of the DAB converter correspond to the ones used in Section V and are described in Table 1. The gains of the controllers, shown in Table 2, have been set according the rules mentioned above, with a desired settling time of 2 ms.

With the initial values of $v(0) = 25$ V, $R_L = 18$ Ω and $P_L = 0$ W, three tests have been simulated: a reference change to a desired value $v_d = 30$ V, a resistive load change to 9 Ω, and finally, a 108 W CPL is connected (disconnecting the resistive load). The simulation has been run at a fixed step size of $1 \cdot 10^{-8}$ s with the ode4 (Runge-Kutta) solver.

Figures from 5 to 8 show the simulation results. The simulations of the TA exhibits the expected performance when using the averaged model, with finite-time convergence and robustness against load changes, see Figure 5. When the algorithm is implemented with the switched model the voltage oscillates around the regulation point with low frequency. This phenomena appears when the sampling of the gate signals is included in the switched model. Low frequency oscillations have been studied when implementing SMC with the use of the Describing Function method [26]. However, in this case the analysis turns to be more complicated because the nonlinear switched system (1a)-(1b) with (2a)-(2b).

The use of the FO sliding-mode controller is shown in Figure 6. As expected, the output voltage behaves as a first

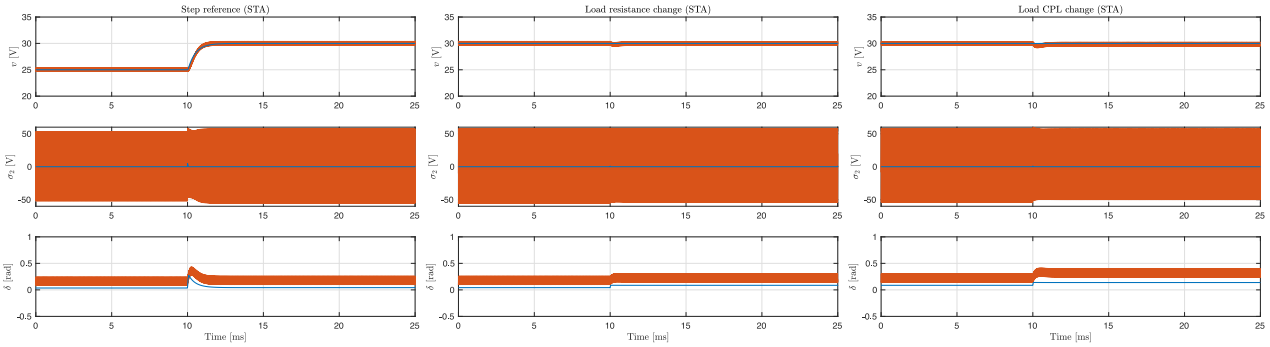

FIGURE 8. Simulation results for the Super Twisting Algorithm (STA): Averaged model (blue), switched model (red). Reference change (left), resistive load change (center), and CPL change (right). Output voltage (top), switching manifold (mid), and phase-shift control signal (bottom).

order system, with the desired time constant of τ, see (8). The asymptotic convergence is the main difference between FO and TA when applied to the averaged model. When the FO controller is tested with the switched model, the behaviour remains close to the one exhibit with the averaged model. The small differences and the overshoot in the response are due to the sampling time of β_A, β_B. The chattering phenomena when using both TA and FO schemes becomes masked by the intrinsic switching of signals β_A, β_B.

The third test evaluates the DIC. The tuning procedure for this algorithm is complicated and the best performance obtained is shown in Figure 7, with a good rejection of load changes but a settling time of 20 ms. Moreover, the algorithm does not stabilize when is tested with the switched model.

Finally, the behaviour of the STA is shown in Figure 8. Similarly to the FO strategy, also based on σ_2, the voltage is regulated with a first-order response with the desired time constant. The controller provides robustness against changes of resistive loads and CPLs. The behaviour is similar when it is applied to the averaged model and the switched model.

V. EXPERIMENTAL RESULTS

The experimental prototype consists of an isolated dc-dc DAB converter with a high-frequency transformer having a unity turns ratio. The parameters of the DAB converter are shown in Table 1. The control strategies were implemented in a TMS320F28377D floating point DSP of Texas Instrument. The power switches used in the converter are IRFP260 MOSFETs. The CPL consists of a dc-dc buck converter with a resistive load of 4.5 Ω. The output voltage is controlled with 22V achieving a constant power of 108 W. Figure 9 shows a picture of the experimental prototype.

The same tests performed for the numerical simulations have been carried out experimentally, for the TA, FO and STA control approaches. As predicted in the simulation stage, the DIC scheme does not stabilize the voltage and it is not included in this section. The gains for all control strategies are the same as the simulation tests given by Table 2.

Figure 10 shows the performance of the output voltage, v, and the phase-shift control signal, δ, for the TA scheme. Similarly to the simulation tests with the switched model, the sampling related to the gate signals result in low-frequency

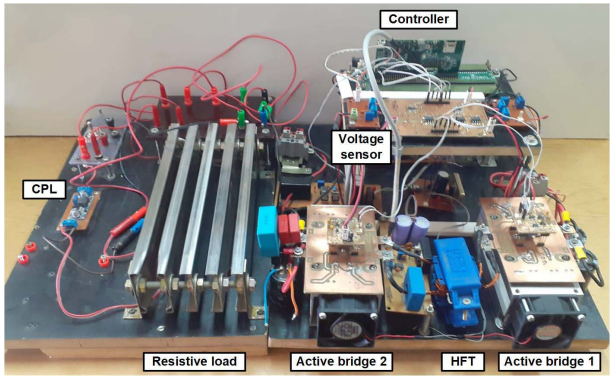

FIGURE 9. Experimental prototype.

oscillations. The amplitude of the oscillations is smaller than the one obtained in the simulations because of unmodelled losses in the DAB components.

The experimental results with the FO controller are presented in Figure 11. In the first plot (left) can be observed how the output voltage, starting at 25 V, reaches the new reference value of 30 V in the desired time (2 ms) following a first-order response, as designed in (9). The second plot (centre) shows the output voltage when the resistive load changes from 18 Ω to 9 Ω. After a short transient, the voltage recovers the desired value. Finally, the third plot (right) confirms the robustness of the FO algorithm in face of CPL connection. Notice that the simulations performed with the switched model in Section IV match to the results with the prototype. The overshoot observed in the numerical simulations is unnoticed in the experimental tests because of the unmodelled losses.

Figure 12 shows the results with the STA. The obtained performance is similar to the one obtained for the FO scheme, and also matches with the simulation tests. Is worth noticing that the STA rejects better the load changes than the FO algorithm, see centre and left plots. Similar waveforms for the current and voltage are obtained using TA and STA, and for this reason they are not included in this section.

Figure 13 shows a detail of the high-frequency transformer current and output voltage for the FO sliding-mode controller. The reference voltage is 30 V and the system is feeding the CPL. It can be observed that in steady-state the output voltage

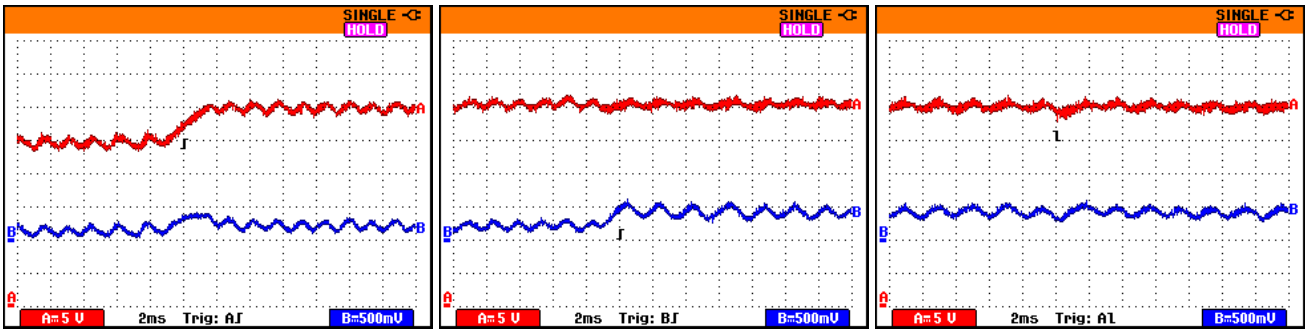

FIGURE 10. Output voltage v (red) and phase-shift control signal δ (blue, scale: 1 rad/V) for the TA. Voltage reference change (left), resistive load change (centre), CPL connection (right).

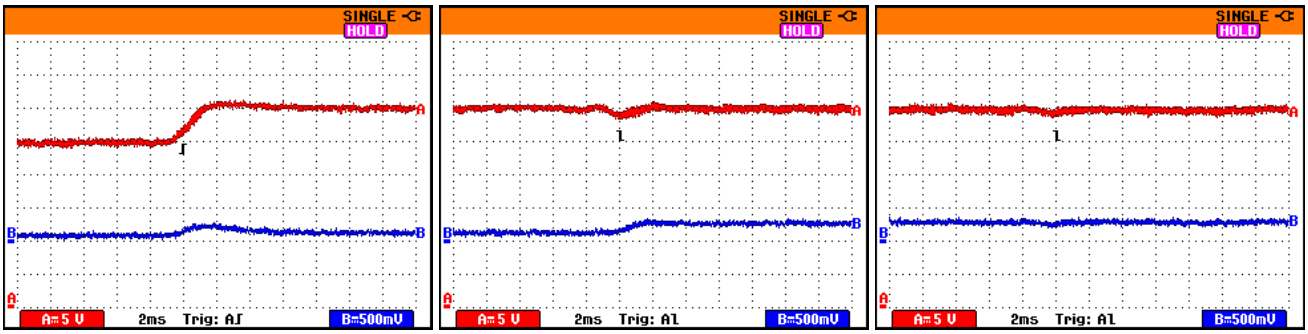

FIGURE 11. Output voltage v (red) and phase-shift control signal δ (blue, scale: 1 rad/V) for the FO sliding-mode controller. Voltage reference change (left), resistive load change (centre), CPL connection (right).

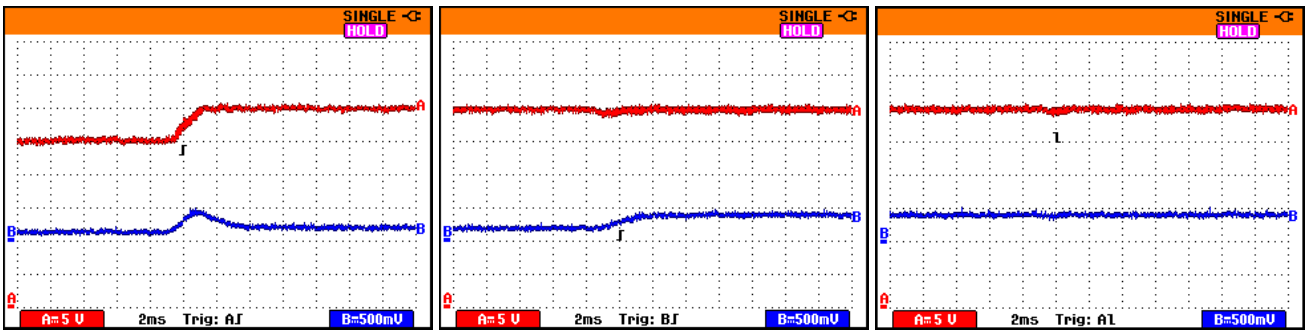

FIGURE 12. Output voltage v (red) and phase-shift control signal δ (blue, scale: 1 rad/V) for the STA. Voltage reference change (left), resistive load change (centre), CPL connection (right).

is regulated to the reference value and the high-frequency transformer current has a mean value equal to zero which prevents the magnetic saturation of the transformer.

Finally, the computational burden of each control scheme is compared. Table 3 shows the execution time of each control routine. Thanks to the simplicity, FO spends less time than TA and STA, using also less computing resources.

TABLE 3. Execution times for each control strategy.

Strategy	Time
TA	480 ns
FO	400 ns
STA	600 ns

VI. EVALUATION DISCUSSION

The comparison of the controllers is performed according to the following indicators:

- Stability accuracy: indicates how accurate is the stability proof concerning the assumptions made along the control design. The DIC and STA need to assume small variations on γ, but TA and FO just need a bound of γ.
- Gain tuning: indicates how difficult is to set the control parameters. The FO is the scheme with easiest tuning with only two parameters. The TA and STA have two and three control parameters, respectively, but rules for STA are more complex. Finally, the tuning of DIC results the more complicated.
- DSP implementation: evaluates the coding into the DSP for its implementation. All the schemes require of a time derivative. The TA and FO only needs the sign function, but the DIC and STA schemes also contain math functions such as the absolute value and fractional exponents.

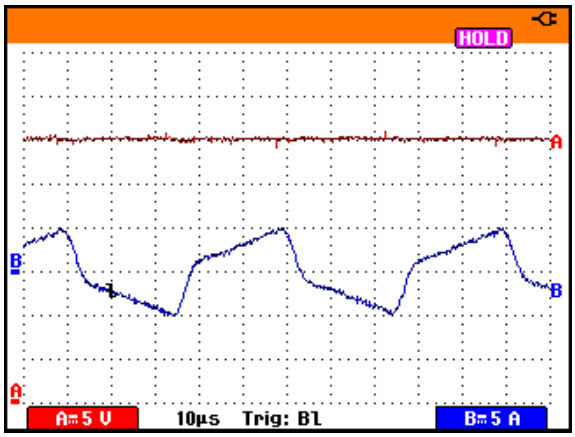

FIGURE 13. Output voltage (red) and high-frequency transformer current (blue) for the FO sliding-mode controller when the CPL is connected.

- Performance: indicates the behaviour of the output voltage from the expected dynamics. Both FO and STA regulate the voltage at the desired value with the expected transient. STA still performs better in simulations. However, with the TA, the oscillations do not allow for regulating the voltage at a constant value. Finally, the DIC only stabilize in simulations with the averaged model.
- Robustness: this indicator evaluates the behaviour in front of load changes. In the experimental stage, the STA is less sensitive to the load variations than the FO.
- Computational burden: evaluates the time required for running the control algorithm. The computational burden of the FO algorithm is lower than more complex strategies such as TA and STA.

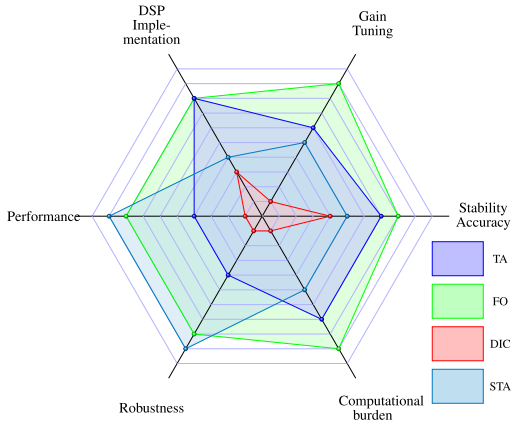

FIGURE 14. Spider chart for an illustrative comparison among the different sliding-mode controllers.

Each control scheme has been graded for each indicator (1 is very poor, 10 is excellent). The results are represented in the spider chart in Figure 14. The conclusion is that the FO and STA are suitable for the control of a DAB, with similar performance. The FO turns to be easiest in the implementation and the gain tuning stage.

VII. CONCLUSION

Four control schemes based on sliding-modes have been proposed for a DAB. A significant difference compared to other control algorithms available in the literature is the use of a dynamic extension to overcome the structural problem of the nonlinear function of the input and redefine the control system affine with the control input. In contrast with other approaches, this alternative does not approximate (or linearize) the function nor use a change of variables requiring more computational resources.

The four alternatives arise from the definition of two different switching functions (resulting in first- and second-order sliding-mode strategies) combined with discontinuous and continuous approaches. All the algorithms have been tested through numerical simulations, and three of them have been experimentally validated.

From a practical point of view, the FO and STA schemes offer excellent regulation performance and robustness properties. In opposite, the second-order approaches are more sensitive to the sampling and discretization stages necessary for the implementation, resulting in undesired oscillations (TA) and instability (DIC).

REFERENCES

[1] F. D. Esteban, F. M. Serra, and C. H. De Angelo, "Control of a DC-DC dual active bridge converter in DC microgrids applications," *IEEE Latin Amer. Trans.*, vol. 19, no. 8, pp. 1261–1269, Aug. 2021.

[2] Q. Xiao, L. Chen, H. Jia, P. W. Wheeler, and T. Dragičević, "Model predictive control for dual active bridge in naval DC microgrids supplying pulsed power loads featuring fast transition and online transformer current minimization," *IEEE Trans. Ind. Electron.*, vol. 67, no. 6, pp. 5197–5203, Jun. 2020.

[3] F. Krismer and J. W. Kolar, "Accurate small-signal model for the digital control of an automotive bidirectional dual active bridge," *IEEE Trans. Power Electron.*, vol. 24, no. 12, pp. 2756–2768, Dec. 2009.

[4] A. Russo, G. Canciello, and A. Cavallo, "Generalized super-twisting control of a dual active bridge for more electric aircraft," in *Proc. Eur. Control Conf. (ECC)*, Jun. 2021, pp. 1610–1615.

[5] S. Inoue and H. Akagi, "A bidirectional DC–DC converter for an energy storage system with galvanic isolation," *IEEE Trans. Power Electron.*, vol. 22, no. 6, pp. 2299–2306, Nov. 2007.

[6] H. Qin and J. W. Kimball, "Closed-loop control of DC–DC dual-active-bridge converters driving single-phase inverters," *IEEE Trans. Power Electron.*, vol. 29, no. 2, pp. 1006–1017, Feb. 2014.

[7] B. Zhao, Q. Yu, and W. Sun, "Extended-phase-shift control of isolated bidirectional DC-DC converter for power distribution in microgrid," *IEEE Trans. Power Electron.*, vol. 27, no. 11, pp. 4667–4680, Nov. 2012.

[8] R. Griñó and A. Dòria-Cerezo, "Modelling and simulation of a magnetically coupled multiport DC-DC converter," in *Proc. 24th IEEE Int. Conf. Emerg. Technol. Factory Autom. (ETFA)*, Sep. 2019, pp. 481–487.

[9] B. P. Baddipadiga and M. Ferdowsi, "Dual loop control for eliminating DC-bias in a DC-DC dual active bridge converter," in *Proc. 3rd Int. Conf. Renew. Energy Res. Appl.*, 2014, pp. 490–495.

[10] D. Das, S. Mishra, and B. Singh, "Design architecture for continuous-time control of dual active bridge converter," *IEEE J. Emerg. Sel. Topics Power Electron.*, vol. 9, no. 3, pp. 3287–3295, Jun. 2021.

[11] D.-D. Nguyen, D.-H. Nguyen, M. Ta, and G. Fujita, "Sensorless feedforward current control of dual-active-bridge DC/DC converter for micro-grid applications," *IFAC-PapersOnLine*, vol. 51, no. 28, pp. 333–338, 2018.

[12] M. Cupelli, S. K. Gurumurthy, S. K. Bhanderi, Z. Yang, P. Joebges, A. Monti, and R. W. De Doncker, "Port controlled Hamiltonian modeling and IDA-PBC control of dual active bridge converters for DC microgrids," *IEEE Trans. on Ind. Electron.*, vol. 66, no. 11, pp. 9065–9074, Nov. 2019.

[13] R. V. Meshram, M. Bhagwat, S. Khade, S. R. Wagh, A. M. Stankovic, and N. M. Singh, "Port-controlled phasor Hamiltonian modeling and IDA-PBC control of solid-state transformer," *IEEE Trans. Control Syst. Technol.*, vol. 27, no. 1, pp. 161–173, Jan. 2019.
[14] I. Askarian, S. Bagawade, M. Pahlevani, A. M. Knight, and A. Bakhshai, "Robust digital nonlinear control system for dual active bridge (DAB) DC/DC converters with asymmetric half-cycle modulation," *IEEE J. Emerg. Sel. Topics Ind. Electron.*, vol. 1, no. 2, pp. 123–132, Oct. 2020.
[15] E. L. S. da Silva, A. L. Kirsten, and D. J. Pagano, "Discrete SPS control of a DAB converter using partial feedback linearization," in *Proc. IEEE 15th Brazilian Power Electron. Conf. 5th IEEE Southern Power Electron. Conf. (COBEP/SPEC)*, Dec. 2019, pp. 1–6.
[16] V. Repecho, J. M. Olm, R. Griñó, A. Dòria-Cerezo, and E. Fossas, "Modelling and nonlinear control of a magnetically coupled multiport DC-DC converter for automotive applications," *IEEE Access*, vol. 9, pp. 63345–63355, 2021.
[17] A. Dòria-Cerezo, F. M. Serra, D. Biel, and R. Griñó, "Sliding mode control of a DC-DC dual active bridge using the generalized space-state averaging description," in *Proc. Eur. Control Conf. (ECC)*, Jun. 2021, pp. 1628–1633.
[18] Y.-C. Jeung and D.-C. Lee, "Voltage and current regulations of bidirectional isolated dual-active-bridge DC–DC converters based on a double-integral sliding mode control," *IEEE Trans. Power Electron.*, vol. 34, no. 7, pp. 6937–6946, Jul. 2019.
[19] J. A. Mueller and J. W. Kimball, "An improved generalized average model of DC–DC dual active bridge converters," *IEEE Trans. Power Electron.*, vol. 33, no. 11, pp. 9975–9988, Nov. 2018.
[20] B. Karanayil, M. Ciobotaru, and V. G. Agelidis, "Power flow management of isolated multiport converter for more electric aircraft," *IEEE Trans. Power Electron.*, vol. 32, no. 7, pp. 5850–5861, Jul. 2017.
[21] A. Levant, "Sliding order and sliding accuracy in sliding mode control," *Int. J. Control*, vol. 58, no. 6, pp. 1247–1263, Dec. 1993.
[22] V. Utkin, J. Guldner, and J. Shi, *Sliding Mode Control in Electro-Mechanical Systems*. Boca Raton, FL, USA: CRC Press, 1999.
[23] J. A. Moreno, "Discontinuous integral control for systems with relative degree two," in *New Perspectives and Applications of Modern Control Theory*. Cham, Switzerland: Springer, 2018, pp. 187–218.
[24] A. Levant, "Robust exact differentiation via sliding mode technique," *Automatica*, vol. 34, no. 3, pp. 379–384, Mar. 1998.
[25] J. A. Moreno and M. Osorio, "A Lyapunov approach to second-order sliding mode controllers and observers," in *Proc. 47th IEEE Conf. Decis. Control*, Dec. 2008, pp. 2856–2861.
[26] U. Pérez-Ventura and L. Fridman, "When is it reasonable to implement the discontinuous sliding-mode controllers instead of the continuous ones? Frequency domain criteria," *Int. J. Robust Nonlinear Control*, vol. 29, no. 3, pp. 810–828, 2018.

ARNAU DÒRIA-CEREZO was born in Barcelona, Spain, in 1974. He received the D.E.A. degree in industrial automation from the Institut National des Sciences Appliqueés de Lyon, Villeurbanne, France, in 2001, and the bachelor's degree in electromechanical engineering and the Ph.D. degree in advanced automation and robotics from the Universitat Politècnica de Catalunya (UPC), Barcelona, in 2001 and 2006, respectively.

He is currently an Associate Professor with the Department of Electrical Engineering, UPC, and carries on his research activities with the Advanced Control of Energy Systems Group, Institute of Industrial and Control Engineering, UPC. From 2003 to 2004, he was a Control Training Site-Research Fellow with the Laboratoire des Signaux et Systèmes, Supélec, France. In 2010, he was a Visitor with the Technische Universiteit Delft, Delft, The Netherlands. His research interests include modeling and control of electrical systems and automotive applications.

Dr. Dòria-Cerezo has been an Associate Editor for *Control Engineering Practice*, since 2017.

FEDERICO M. SERRA was born in Villa Mercedes, Argentina, in 1981. He received the Electrical and Electronics Engineer degree from the Universidad Nacional de San Luis, Argentina, in 2007, and the Ph.D. degree in engineering science from the Universidad Nacional de Río Cuarto, Argentina, in 2013. He is currently a Professor with the Universidad Nacional de San Luis, the Director of the Engineering Department, and an Adjunct Researcher with the Consejo Nacional de Investigaciones Científicas y Técnicas (CONICET). Since 2012, he has been the Director of the Automatic Control Laboratory (LCA), Universidad Nacional de San Luis. His research interests include modeling and advanced control of power converters in applications of microgrids, electric vehicles, and renewable energy conversion systems.

FRANCISCO D. ESTEBAN was born in Nueve de Julio, Argentina, in 1992. He received the Electronics Engineer degree from the Universidad Nacional de San Luis, Argentina, in 2018. He is currently pursuing the Ph.D. degree in engineering sciences with the Universidad Nacional de Rio Cuarto, Argentina. Since 2014, he has been a member of the Automatic Control Laboratory (LCA), Universidad Nacional de San Luis, where he is also an Auxiliar Professor. His research interests include modeling and control of power converters in applications of microgrids, electric vehicles, and renewable energy conversion systems.

DOMINGO BIEL received the B.S., M.S., and Ph.D. degrees in telecommunications engineering from the Universitat Politècnica de Catalunya (UPC), Barcelona, Spain, in 1990, 1994, and 1999, respectively. Since 1998, he has been an Associate Professor with the Electronic Engineering Department, UPC, where he teaches power electronics and control theory. His research interests include nonlinear control and its application to renewable energy systems and power electronics.

ROBERT GRIÑÓ (Senior Member, IEEE) received the M.Sc. degree in electrical engineering and the Ph.D. degree in automatic control from the Universitat Politècnica de Catalunya (UPC), Barcelona, Spain, in 1989 and 1997, respectively.

From 1990 to 1991, he was a Research Assistant with the Instituto de Cibernética, UPC. From 1992 to 1998, he was an Assistant Professor with the Automatic Control Department, UPC, where he has been an Associate Professor, since 1998. He is currently the Director of the Institute of Industrial and Control Engineering (IOC), UPC. His research interests include digital control, nonlinear control, and control of power electronic converters.

Dr. Griñó is a member of the Spanish Committee of Automatica (CEA-IFAC) and an affiliate of the International Federation of Automatic Control (IFAC) and a member of its Technical Committee 6.3, "Power and Energy Systems."